International Journal of Control, Automation and Systems 16(3) (2018) 994-1010
http://dx.doi.org/10.1007/s12555-017-0362-1
ISSN:1598-6446 eISSN:2005-4092
http://www.springer.com/12555

IMC based Controller Design for Automatic Generation Control of Multi Area Power System via Simplified Decoupling

Idamakanti Kasireddy*, Abdul Wahid Nasir, and Arun Kumar Singh

Abstract: This paper deals with design of integer and non-integer IMC based controllers for automatic generation control of two area power system using the simplified decoupling technique. A two area non-reheated interconnected thermal power system is considered for decentralised controller design. The coupling among areas are the main hurdle encountered in the design of controller. Hence, the idea of simplified decoupling technique is introduced to decouple the two area power system into two equivalent independent SISO systems. Integer and non-integer internal model control (IMC), are independently designed for each area based on decoupled systems. The performance of two area power system equipped with proposed controller is analysed through MATLAB. Simulation results show that proposed controller maintains robust performance and can minimize the load fluctuations. Finally, the method is extended to three area power system.

Keywords: Automatic generation control(AGC), multi area power system, simplified decoupling, genetic algorithm, internal model control (IMC).

1. INTRODUCTION

In an electric power system, different regions are interconnected through transmission lines which are known as tie lines. Power exchanging between any two regions is possible through tie lines. Each region is equipped with different generators and loads. All generators in each region are operated synchronously at the same frequency to meet required demand power. If any power imbalance occurs between generators and loads, then that reflects in terms of frequency deviation and tie line power deviation. The imbalance may be due to random load fluctuations or due to power plant tripping out, faults etc. The power generated by generators is more than connected load, which causes the frequency rise or machine acceleration. Similarly, the power generated by generators is less than demand power, which causes the frequency fall or machine deceleration. This change in frequency is the reason for the motor speed variations, increase in harmonic currents, change in magnetizing current in transformers, etc.. Hence the main objective is to maintain the frequency and tie line power exchange at pre-specified ranges [1, p. 581-582], [2, p. 291], [3, pp. 310]. This can be achieved through secondary controller as AGC in addition to the governor. To design a secondary controller, the interconnected power system is modelled and simulated.

In [4, 5], an extensive review on different control techniques and strategies for load frequency control (LFC) of different power system models has been highlighted. At first, the AGC design of power system was based on centralized control strategy. But it is well known that a lot of computation & communication is involved in AGC which is based on centralized control scheme. These complexities of computation & communication can be greatly reduced if decentralized scheme of control is adopted in AGC. In [6], the robust decentralized proportional integral (PI) based LFC is designed for three area power system with communication delay. [7] discussed decentralized neural network based LFC of three area deregulated power system. [8] proposed a robust proportional-integral-derivative (PID) controller design for perturbed four area power system model. [9] presented a robust decentralized controller for LFC of multi area power system. [10] studied an adaptive fuzzy based LFC of the interconnected power system. A decentralized sliding mode controller for LFC of multi area power system has been discussed in [11]. [12] studied an adaptive decentralized LFC for the interconnected power system.

From literature survey, it can be observed that multi area power system is having coupling dynamics among the areas through tie lines. As a result, the secondary controller output affects the dynamics of other areas. Thus the coupling dynamics is the main hurdle encountered while designing the decentralized controller. In this work, the concept of simplified decoupling [13, pp. 437-438] is employed to eliminate the coupling dynamics among the ar-

Manuscript received June 21, 2017; revised September 21, 2017 and November 6, 2017; accepted November 20, 2017. Recommended by Associate Editor Young Ik Son under the direction of Editor Euntai Kim.

Idamakanti Kasireddy, Abdul Wahid Nasir, and Arun Kumar Singh are with the Department of Electrical and Electronics Engineering, NIT Jamshedpur, 831014, India (e-mails: 2015rsee002@nitjsr.ac.in, awonasir@gmail.com, aksnitjsr@gmail.com).
* Corresponding author.

eas in two area power system for controller design. The main advantage of simplified decoupling is that independent single-input single-output (SISO) systems can be achieved. Internal model control (IMC) is one of the robust control methods and is easy to implement for SISO systems [14–16]. Recently, the concept of fractional calculus and its applications in control theory have significantly increased. From literature, the integer operators of conventional control methods have been replaced by the concept of fractional calculus [17–19]. In this paper, integer and non-integer IMC controllers are designed based on measurement of frequency deviation(Δf_i), a local variable for each obtained SISO models. Further the two area power system is equipped with proposed controller and is simulated in MATLAB. The performance of proposed controller is examined under wide variations of system parameters. Also, it is tested against a random load perturbation that may match with real time load profile. The simulation results are compared with Wen Tan method [20] for similar power system, which showed the superiority of the proposed design approach. The applicability of the proposed method is also tested for the extension of the power system from two area to three area system through different MATLAB simulations. For carrying the simulation work related to different non-integer system, FOMCON [21] is used.

This paper is segregated into the following sections. Simplified decoupling method of two area power system is discussed in Section 2. The design of integer and non-integer IMC controller is discussed in Section 3. Section 4 illustrates the analysis of designed controllers against load disturbance and system parameter variations. Section 5 discussed the applicability of proposed method to three area power system. Finally, the conclusions are addressed in section 6.

2. SIMPLIFIED DECOUPLING FOR MULTI AREA POWER SYSTEM

This section works on obtaining of SISO models for two area non-reheated interconnected power system using simplified decoupling. This is divided into subsections as follows.

2.1. Two area power system

In general the models of governor, turbine and power system are non linear. But these models usually represented by linearised models around an operating point for LFC study. Under normal operating condition, the power system is exposed to a small perturbation, hence their linear models will work good to mimic the dynamic of non-linear models [22], [12]. Due to the simplicity of frequency domain analysis as compared to time domain, the linearised models of the system are represented by transfer functions. Fig. 1 shows the transfer function

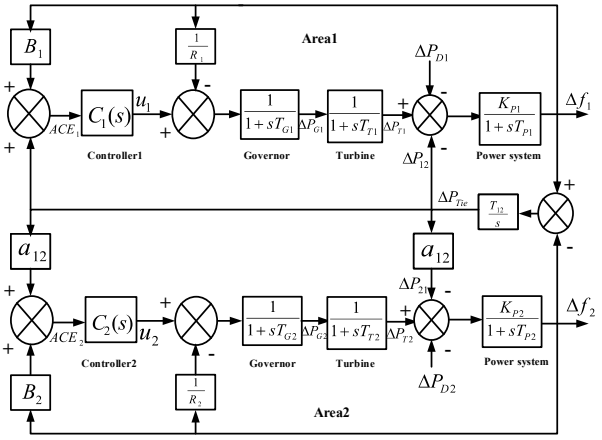

Fig. 1. Two area power system model under study.

model of a two area power system [20, 23]. Each area equipped with non-reheated turbine, governor and power system linear models. Two areas are connected through a tie line through which power exchange among the areas takes place.

The governor dynamics can be represented by transfer function [3]:

$$G_G(s) = \frac{1}{T_G s + 1}. \tag{1}$$

The turbine dynamics can be represented by transfer function [3]:

$$G_T(s) = \frac{1}{T_T s + 1}. \tag{2}$$

The power system dynamics can be represented by transfer function [3]:

$$G_P(s) = \frac{K_P}{T_P s + 1}, \tag{3}$$

where $K_P = 1/D$ and $T_P = 2H/fD$. The tie line exchange power ΔP_{tie} is given by (4) [3, pp. 330-331]

$$\Delta P_{tie} = \frac{T_{12}}{s}(\Delta f_1 - \Delta f_2) \tag{4}$$

where T_{12} is synchronizing power coefficient. From Fig. 1, $ACE_i (i = 1,2)$ is defined as a linear combination of frequency deviation and tie line interchange power and is given by (5)

$$ACE_1 = \Delta P_{tie} + B_1 \Delta f_1, ACE_2 = a_{12}\Delta P_{tie} + B_2 \Delta f_2, \tag{5}$$

where B_1, B_2 are the frequency bias settings.

A 2×2 model from u_i to Δf_i, (i=1,2) is obtained [20] as below.

From Fig. 1, we have

$$\Delta f_1 = G_{P1}(s)G_{T1}(s)G_{G1}(s)(u_1 - \Delta f_1/R_1)$$

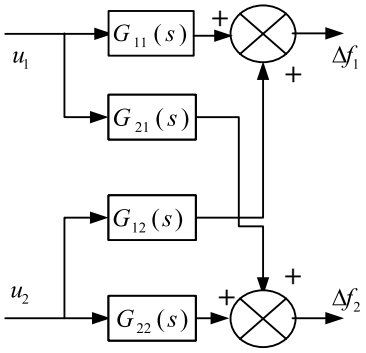

Fig. 2. Representation of coupled TITO system.

$$
\begin{aligned}
&-G_{P1}(s)(\Delta f_1-\Delta f_2)T_{12}/s-\Delta P_{D1},\\
\Delta f_2 = {}& G_{P2}(s)G_{T2}(s)G_{G2}(s)(u_2-\Delta f_2/R_2)\\
&-G_{P2}(s)(\Delta f_1-\Delta f_2)T_{12}/s-\Delta P_{D2}.
\end{aligned}
$$

Rearranging above equations into matrix form and ΔP_{D1} & ΔP_{D2} are set to zero(assuming no load disturbance). The resultant matrix is obtained as (6)

$$
\begin{aligned}
&\begin{bmatrix}\Delta f_1\\ \Delta f_2\end{bmatrix}\\
&=\begin{bmatrix}L & -G_{P1}(s)T_{12}/s\\ -G_{P2}(s)T_{12}/s & M\end{bmatrix}^{-1}\\
&\quad\times\begin{bmatrix}G_{P1}(s)G_{T1}(s)G_{G1}(s) & 0\\ 0 & G_{P2}(s)G_{T2}(s)G_{G2}(s)\end{bmatrix}\begin{bmatrix}u_1\\ u_2\end{bmatrix},
\end{aligned}
\tag{6}
$$

where

$$
L = 1+G_{P1}(s)G_{T1}(s)G_{G1}(s)/R_1+G_{P1}(s)T_{12}/s, \tag{7a}
$$

$$
M = 1+G_{P2}(s)G_{T2}(s)G_{G2}(s)/R_2+G_{P2}(s)T_{12}/s. \tag{7b}
$$

Equation (6) shows that off diagonal elements are non-zeros, shows the coupling effect among the areas which can be represented by Fig. 2, where $G_{11}(s)$, $G_{12}(s)$, $G_{21}(s)$ and $G_{22}(s)$ are the simplified estimated models relating input u_1 and output Δf_1, input u_1 and output Δf_2, input u_2 and output Δf_1, and input u_2 and output Δf_2 respectively. The parameter estimation of these models have been under taken in section 2.3. Therefore, the (6) is simplified as follows.

$$
\begin{bmatrix}\Delta f_1\\ \Delta f_2\end{bmatrix}=\begin{bmatrix}G_{11}(s) & G_{12}(s)\\ G_{21}(s) & G_{22}(s)\end{bmatrix}\begin{bmatrix}u_1\\ u_2\end{bmatrix}. \tag{8}
$$

In Fig. 1, u_1 and u_2 are the control outputs from the controller; R_1 and R_2 are the governor speed regulation parameters in p.u. Hz; T_{G1} and T_{G2} are the speed governor time constants in sec; ΔP_{G1} and ΔP_{G2} are the governor output command (p.u.); T_{T1} and T_{T2} are the turbine time constant in sec; ΔP_{T1} and ΔP_{T2} are the change in turbine output powers; ΔP_{D1} and ΔP_{D2} are the load demand changes; ΔP_{tie} is the incremental change in tie line power (p.u.); K_{P1} and K_{P2} are the power system gains; T_{P1} and T_{P2} are the power system time constant in sec; and Δf_1 and Δf_2 are the system frequency deviations in Hz. Nominal parameters of the system are [20]

$f = 60Hz$; $B_1, B_2 = 0.045$; $R_1, R_2 = 2.4Hz/p.u$; $T_{G1}, T_{G2} = 0.08s$; $T_{T1}, T_{T2} = 0.3s$; $a_{12} = -1$;$K_{P1}, K_{P2} = 120Hz/p.uMw$; $T_{P1}, T_{P2} = 20s$.

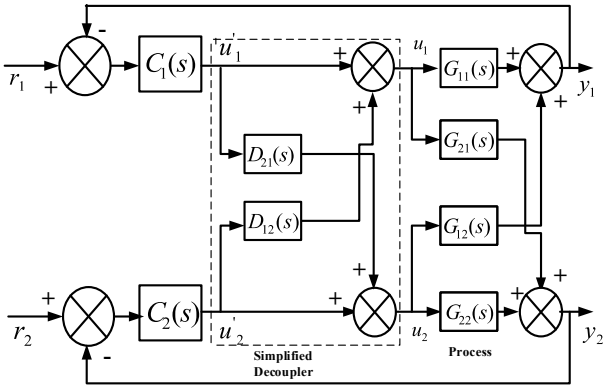

Fig. 3. Block diagram of simplified decoupling.

2.2. Simplified decoupling

This subsection introduces a simplified decoupling method which helps to decouple the two area power system into two equivalent independent systems.

The simplified decoupling of a two input two output (TITO) system is shown in Fig. 3. Luyben [24] introduced the simplified decoupling and this method is widely used in literature [25–28]. The idea of decoupling is to find a decoupler matrix $D(s)$ so that $G(s)D(s) = G^*(s)$ is a diagonal matrix.

Consider the TITO system and is represented by (9)

$$
G(s)=\begin{bmatrix}G_{11}(s) & G_{12}(s)\\ G_{21}(s) & G_{22}(s)\end{bmatrix}. \tag{9}
$$

Selecting [13] a decoupler matrix as

$$
D(s)=\begin{bmatrix}1 & D_{12}(s)\\ D_{21}(s) & 1\end{bmatrix}, \tag{10}
$$

where

$$
D_{12}(s)=\frac{-G_{12}(s)}{G_{11}(s)}, \tag{11}
$$

and

$$
D_{21}(s)=\frac{-G_{21}(s)}{G_{22}(s)}. \tag{12}
$$

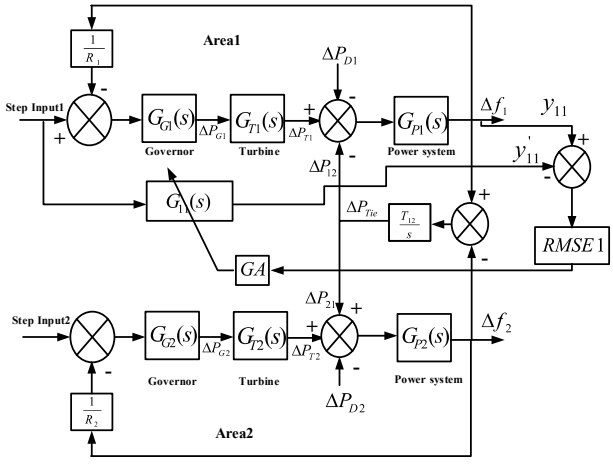

Fig. 4. Parameter estimation of transfer function G_{11} model.

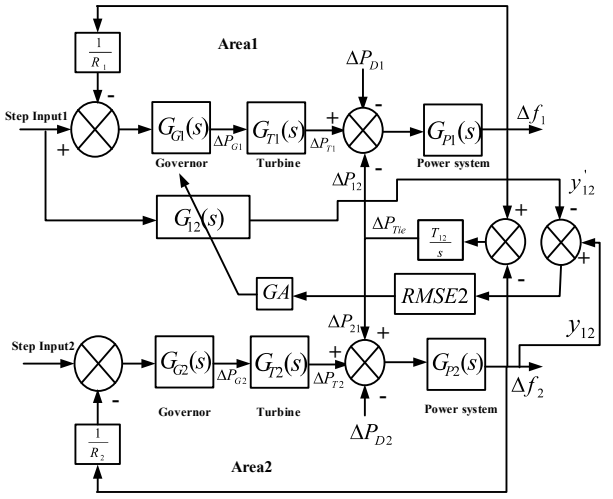

Fig. 5. Parameter estimation of transfer function G_{12} model.

Then the resulting matrix $G^*(s)$ is obtained as

$$\begin{aligned} G^*(s) &= \begin{bmatrix} G_{11}^*(s) & 0 \\ 0 & G_{22}^*(s) \end{bmatrix} \\ &= \begin{bmatrix} G_{11}(s) & G_{12}(s) \\ G_{21}(s) & G_{22}(s) \end{bmatrix} \begin{bmatrix} 1 & D_{12}(s) \\ D_{21}(s) & 1 \end{bmatrix} \qquad (13) \\ &= \begin{bmatrix} G_{11}(s)+G_{12}(s)D_{21}(s) & G_{11}(s)D_{12}(s)+G_{12}(s) \\ G_{21}(s)+G_{22}(s)D_{21}(s) & G_{21}(s)D_{12}(s)+G_{22}(s) \end{bmatrix}, \qquad (14) \end{aligned}$$

substituting $D_{12}(s) = \dfrac{-G_{12}(s)}{G_{11}(s)}$ & $D_{21}(s) = \dfrac{-G_{21}(s)}{G_{22}(s)}$ in (14) and resultant is given by (15)

$$G^*(s) = \begin{bmatrix} G_{11}(s) - \dfrac{G_{12}(s)G_{21}(s)}{G_{22}(s)} & 0 \\ 0 & G_{22}(s) - \dfrac{G_{12}(s)G_{21}(s)}{G_{11}(s)} \end{bmatrix}. \qquad (15)$$

2.3. System identification

In order to make use of decoupling technique, the two area power system is simplified in the form of Fig. 2 using output error (OE) identification method. Since the dynamics of real system is complex, hence OE identification is employed to estimate much simpler model which replicates the input-output behaviour of real system [29–34].

The two area power system model is approximated using different types of models. Through extensive simulations it was found that the nature of the transfer function relating the Area 1 input(u_1) & Area 1 output(Δf_1) represented by $G_{11}(s)$ is given by (16).

$$G_{11}(s) = \frac{(k_1 s + k)e^{-L_1 s}}{as^3 + bs^2 + cs + 1}. \qquad (16)$$

Similarly, transfer function relating the Area 1 input(u_1) & Area 2 output(Δf_2) represented by $G_{12}(s)$ is given by (17)

$$G_{12}(s) = \frac{kke^{-L_2 s}}{aas^3 + bbs^2 + ccs + 1}, \qquad (17)$$

where L_1 and L_2 are time delay of $G_{11}(s)$ and $G_{12}(s)$ respectively.

For simplicity, both the areas are assumed to be identical [20, 23] as shown in Fig. 1. Hence, $G_{21}(s)$ and $G_{22}(s)$ can be represented as

$$G_{22}(s) = G_{11}(s) \text{ and } G_{21}(s) = G_{12}(s).$$

The parameters of these estimated models are unknown, and OE identification is employed to identify the unknown parameters. The steps for identifying estimated model $G_{11}(s)$ are as follows:

Step 1: A step input is given to Area 1 while input to Area 2 is zero and output y_{11} is obtained. The corresponding system is shown in Fig. 4.

Step 2: Similarly a step input is given to system $G_{11}(s)$ constructed by assigning probable parameters and output y'_{11} is obtained.

Step 3: The output y_{11} and y'_{11} are compared and their difference is passed to a performance index RMSE which evaluates the performance of assigned parameters in representing real system.

Step 4: Again new parameters are updated to $G_{11}(s)$ and simulated in similar as from steps 1, 2, 3 until the best solution is obtained. The parameters generation of

$$\begin{bmatrix}\Delta f_1\\ \Delta f_2\end{bmatrix} = \begin{bmatrix}\dfrac{(2.864s+1.1766)e^{-0.0497s}}{0.155s^3+0.532s^2+1.6957s+1} & \dfrac{1.1767e^{-0.2715s}}{0.1673s^3+0.33s^2+1.342s+1}\\ \dfrac{1.1767e^{-0.2715s}}{0.1673s^3+0.33s^2+1.342s+1} & \dfrac{(2.864s+1.1766)e^{-0.0497s}}{0.155s^3+0.532s^2+1.6957s+1}\end{bmatrix}\begin{bmatrix}u_1\\ u_2\end{bmatrix} \tag{20}$$

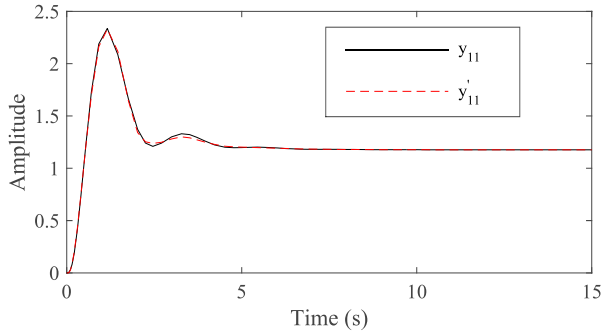

Fig. 6. Comparison of y_{11} and y'_{11} step responses.

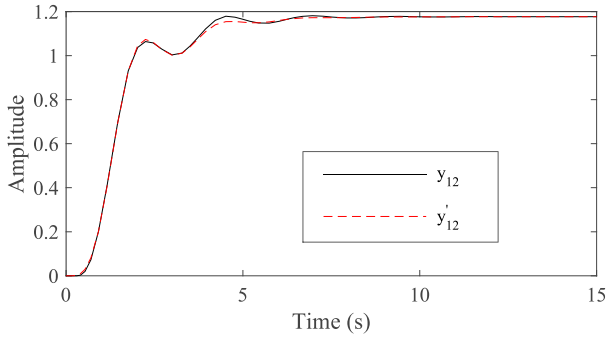

Fig. 7. Comparison of y_{12} and y'_{12} step responses.

$G_{11}(s)$ is done by heuristic algorithms which is a genetic algorithm(GA) in present case.

where RMSE is the root mean squared error performance index and is denoted by J, which is defined as (18).

$$J = RMSE = \sqrt{\frac{e_1^2+e_2^2+\ldots+e_n^2}{n}}. \tag{18}$$

Similarly the system $G_{12}(s)$ as shown in Fig. 5 is obtained using above steps.

The step responses y_{11} and y'_{11} are compared and depicted in Fig. 6 where as y_{12} and y'_{12} are compared and depicted in Fig. 7 . The corresponding RMSE values are obtained as $RMSE1 = 0.0307$ and $RMSE2 = 0.0244$.

The obtained parameters of $G_{11}(s)$ is given as

$$k_1 = 2.864,\ \ k = 1.1766,\ \ L_1 = 0.0497,\ \ a = 0.155,$$
$$b = 0.532,\ \ c = 1.6957.$$

The obtained parameters of $G_{12}(s)$ is given as

$$kk = 1.1767,\ \ L_2 = 0.2715,\ \ aa = 0.17,\ \ bb = 0.33,$$
$$cc = 1.34.$$

The obtained estimated models are given by (19a) and (19b)

$$G_{22}(s) = G_{11}(s) = \frac{(2.864s+1.1766)e^{-0.0497s}}{0.155s^3+0.532s^2+1.6957s+1}, \tag{19a}$$

and

$$G_{21}(s) = G_{12}(s) = \frac{1.1767e^{-0.2715s}}{0.1673s^3+0.33s^2+1.342s+1}, \tag{19b}$$

substitute (19a) and (19b) in (8), then (8) can be simplified as (20) at top of the page.

2.4. Genetic algorithm

GA is developed by John Holland and his co-workers in the year 1960s & in 1970s, which is nature inspired heuristic optimization method [35–38]. It is superior in solving complex problems compared to other optimization algorithms. It can deal with the objective function which may be time varying or time invariant, linear or non-linear, continuous or discrete. In this paper, GA is engaged to find the estimated model parameters.

Initially, a random population of individuals are generated, owning a presumed set of parameters depicting the genes of chromosomes or individuals, to be the possible solution of search space. A fitness function evaluates the fitness of each individuals in the population, which is being minimized or maximized as per need of problem to get optimal solution. The highest fitness value of individuals are selected from present population. And corresponding individuals then undergo the process of mutation and crossover to generate new population with updated fitness value. Based on this updated information, best fitness value of individuals is selected among all the generations. Above process keeps on repeating until a optimal solution is achieved fulfilling the stopping criteria. The flow chart of GA is shown in Fig. 8.

The parameter selection of GA is given in Table 1. The convergence curves of GA for parameter estimation of $G_{11}(s)$ and $G_{12}(s)$ are shown in Fig. 9 and Fig. 10 respectively. It is clear from Fig. 9 and Fig. 10 that, GA converge at about 16-20 generations in both cases.

2.5. Design of proposed system

The technique to decouple the dynamics of two areas is discussed in Subsection 2.2, which is applied to a system

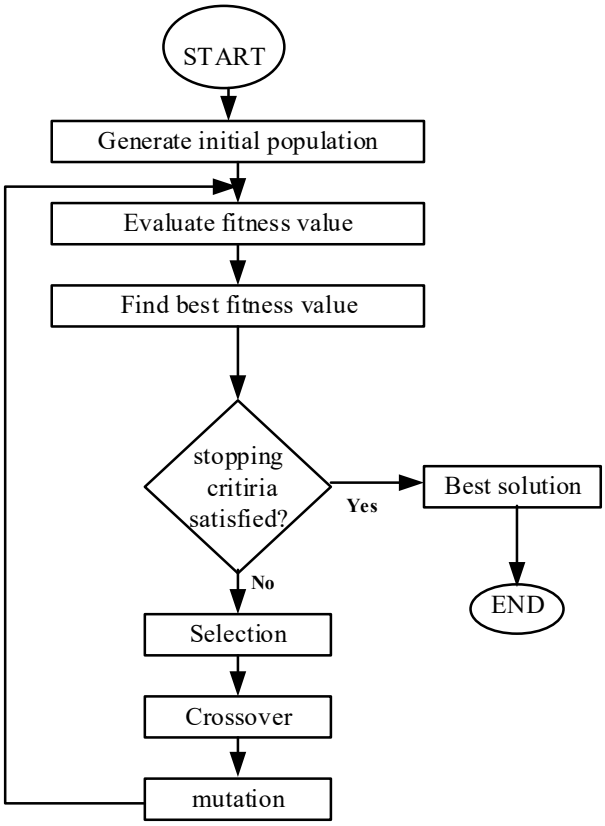

Fig. 8. Flow Chart of GA.

Table 1. Genetic algorithm characteristics.

Parameter selection	
No.of generations	20
Population size	80
Crossover probability	0.5
Mutation probability	0.2
Elite count	4

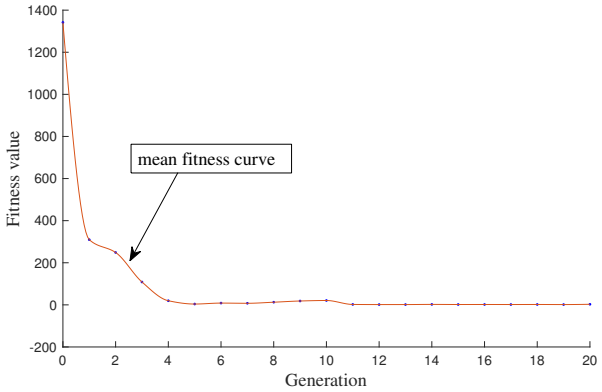

Fig. 9. Convergence curve of the GA for G_{11} parameter estimation.

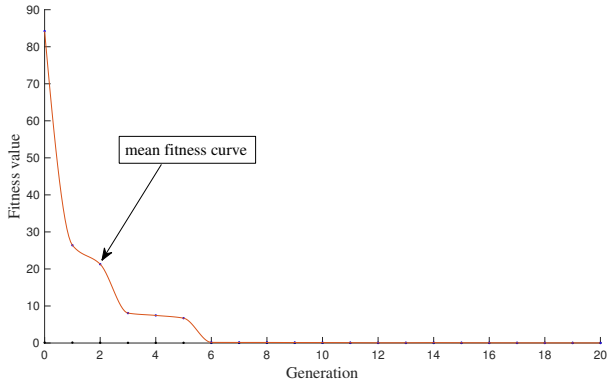

Fig. 10. Convergence curve of the GA for G_{12} parameter estimation.

(20) as shown in Fig. 3, yielding the proposed model.

Substituting the systems $G_{11}(s)$, $G_{12}(s)$, $G_{21}(s)$ and $G_{22}(s)$ in (15), then $G^*(s)$ is simplified as

$$G^*(s) = \begin{bmatrix} G^*_{11}(s) & 0 \\ 0 & G^*_{22}(s) \end{bmatrix}, \tag{21}$$

where

$$G^*_{11}(s) = G^*_{22}(s) = \frac{(4.2922s + 0.394)e^{-0.099s}}{0.203s^3 + 0.658s^2 + 1.49s + 1}, \tag{22}$$

where $G^*_{11}(s)$ and $G^*_{22}(s)$ represent the SISO systems relating Area 1 input(u_1') to Area 1 output(Δf_1)and Area 2 input(u_2') to Area 2 output(Δf_2) respectively. From (21), it is observed that off diagonal elements are zero.

In this LFC or AGC case [8,9,20], decentralized control means that only local measurements(Δf_i) is used for controller design, but later while implementing it ACE signal is taken into consideration instead of only frequency deviation. Thus secondary controller can be tuned independently for each area considered as SISO systems.

3. INTEGER AND NON-INTEGER IMC CONTROLLERS

This section describes the integer and non-integer IMC controllers & its application in AGC of two area power system power system.

3.1. Internal model control

In this subsection an IMC method adopted for secondary controller, which is developed by M.Morari [39, 40]. The block diagram of two degree of freedom (TDF)-IMC structure is shown in Fig. 11,
where

$P(s) =$ Plant to be controlled,
$\bar{P}(s) =$ Model for plant,

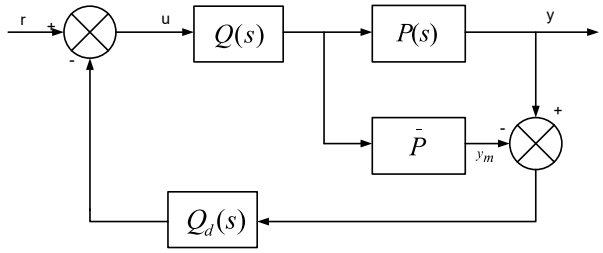

Fig. 11. Block diagram of TDF-IMC.

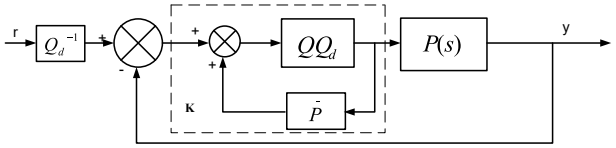

Fig. 12. Equivalent conventional feedback control system.

$Q(s) =$ IMC based controller,
$Q_d(s) =$ Disturbance rejection IMC controller.

The non-integer IMC filter design goes as follows [15];

Step 1: Plant model $\bar{P}(s)$ can be decomposed into two parts;

$$\bar{P}(s) = P^+(s)P^-(s), \tag{23}$$

where

$P^-(s) =$ invertible part,
$P^+(s) =$ non-invertible part
(e.g., time delay, zeros in right side of S-plane etc.).

Step 2: Set point tracking non-integer IMC controller transfer function is consider as

$$Q(s) = \frac{1}{P^-(s)}\frac{1}{(\lambda s^a+1)^r}, \tag{24}$$

where λ, a are the tuning parameters and r is the positive integer, $r \geq 2$. Here r is chosen as 2 so that $Q(s)$ becomes proper. And range of a is $a \geq 1$.

Step 3: The disturbance rejection non-integer IMC controller transfer function is consider as

$$Q_d(s) = \frac{\alpha_m s^m + ... + \alpha_1 s + 1}{(\lambda_d s^b+1)^m}, \tag{25}$$

where λ_d and b are the tuning parameters of and m is number of poles of $\bar{P}(s)$. Here there is constraint on b such that $b \geq 1$, to make $Q_d(s)$ proper. α_1, α_2, ..., α_m are calculated using (26) such that P_1, P_2, ..., P_m are the poles get cancelled.

$$(1-\bar{P}(s)Q(s)Q_d(s))|_{s=P_1,P_2,...P_m} = 0. \tag{26}$$

Fig. 11 can be transformed to conventional closed loop control as shown in Fig. 12, where non-integer feedback controller $K(s)$ is given by (27)

$$K(s) = \frac{Q(s)Q_d(s)}{1-\bar{P}(s)Q(s)Q_d(s)}. \tag{27}$$

Similarly the integer IMC filter design is obtained by simply taking the values a & b as unity i.e., $a = b = 1$.

3.2. Application of integer and non-integer IMC design to two area power system

From (22), the plant to be controlled is

$$P(s) = G^*_{11}(s) = G^*_{22}(s) = \frac{(4.2922s+0.394)e^{-0.099s}}{0.203s^3+0.658s^2+1.49s+1}. \tag{28}$$

Using (23), the invertible part of $P(s)$ is given by (29)

$$P^-(s) = \frac{4.2922s+0.394}{0.203s^3+0.658s^2+1.49s+1}. \tag{29}$$

From (24), set point tracking non-integer IMC controller is given by (30)

$$Q(s) = \frac{1}{P^-(s)}\frac{1}{(\lambda s^a+1)^2}, \tag{30}$$

$$Q(s) = \frac{0.203s^3+0.658s^2+1.49s+1}{(4.2922s+0.394)(\lambda s^a+1)^2}. \tag{31}$$

The frequency $\Delta f(s)$ is affected due to load perturbation ΔP_D, which must passing through $K_P/(T_P s+1)$. To have fast disturbance rejection, we choose $Q_d(s)$ as (32)

$$Q_d(s) = \frac{\alpha_1 s+1}{(\lambda_d s^b+1)}, \tag{32}$$

where $\alpha 1$ is calculated using (33)

$$(1-\bar{P}(s)Q(s)Q_d(s))|_{s=-1/T_P} = 0, \tag{33}$$

substituting $\bar{P}(s), Q(s)$ and $Q_d(s)$ in (33), we get

$$(1-e^{-0.099s}\frac{1}{(\lambda s^a+1)^2}\frac{\alpha_1 s+1}{(\lambda_d s^b+1)})|_{s=-1/T_P} = 0. \tag{34}$$

$$[\lambda(-1/T_P)^a+1]^2[\lambda_d(-1/T_P)^b+1] = (-1.0049\alpha_1/T_P)+1.0049, \tag{35}$$

$$\alpha_1 = T_P[1-0.995[1-\lambda(1/T_P)^a]^2[1-\lambda_d(1/T_P)^b]]. \tag{36}$$

Substitute $Q(s)$, $Q_d(s)$ and $\bar{P}(s)$ in (27), we get non-integer IMC controller with tuning parameters λ, λ_d, a and b. Similarly integer IMC controller is obtained by substituting $Q(s)$, $Q_d(s)$ and $\bar{P}(s)$ in (27) by taking $a = 1$ and $b = 1$. The procedure for tuning of parameters is discussed in Section 4.

Table 2. Comparison of error performance index.

Step disturbance	Non-integer case			Wen Tan case			Integer case		
	ISE1	ISE2	E(%)	ISE1	ISE2	E(%)	ISE1	ISE2	E(%)
ΔP_{D1} =0.05 & ΔP_{D2}=0	0.00027	$1.01*10^{-6}$	0.374	0.0013	0.0002	15.4	0.00076	$5.9*10^{-6}$	0.776
ΔP_{D1} =0.1 & ΔP_{D2}=0	0.001	$4.05*10^{-6}$	0.405	0.0054	0.00075	13.88	0.003	$2.37*10^{-5}$	0.8
ΔP_{D1} =0.5 & ΔP_{D2}=0	0.027	0.0001	0.38	0.14	0.02	14.3	0.076	0.00059	0.78

4. RESULTS AND ANALYSIS

This work aggregates the modelling of two area power system and design of proposed controller. These are achieved in Section 2 and Section 3 while Section 4 demonstrates capability of controller for the proposed system. Using the measurement of Δf_i for each area, IMC based controllers are tuned for each SISO models individually.

The obtained parameter values for the non-integer IMC controller are given below:

$$\lambda = 0.12,\ \ \lambda_d = 0.0001,$$
$$a = 1.02,\ \ b = 1.3,\ \ \alpha_1 = 0.3315.$$

The resulting non-integer IMC controller is given as

$$C_1(s) = C_2(s) = K_{non-int}(s) = \frac{Q(s)Q_d(s)}{1-\bar{P}(s)Q(s)Q_d(s)}, \tag{37}$$

where

$$Q(s) = \frac{0.203s^3+0.658s^2+1.49s+1}{(4.2922s+0.394)(0.12s^{1.02}+1)^2},$$

and

$$Q_d(s) = \frac{0.3315s+1}{(0.0001s^{1.3}+1)}.$$

The obtained parameter values for the integer IMC controller are given below:

$$\lambda = 0.25,\ \ \lambda_d = 0.001 \ \text{ and } \ \alpha_1 = 0.6041.$$

The resulting integer IMC controller is given as

$$C_1(s) = C_2(s) = K_{int}(s) = \frac{Q(s)Q_d(s)}{1-\bar{P}(s)Q(s)Q_d(s)}, \tag{38}$$

where

$$Q(s) = \frac{0.203s^3+0.658s^2+1.49s+1}{(4.2922s+0.394)(0.25s+1)^2},$$

and

$$Q_d(s) = \frac{0.6041s+1}{(0.001s+1)}.$$

The system identification of G_{11} & G_{12} is being carried out in section 2.3 based on RMSE criterion and its values are found to be RMSE1=0.0307 & RMSE2=0.0244 respectively. The effect of these errors on decoupling and controller performance is studied analytically via different simulation results. The step disturbance is introduced in Area 1 while keeping disturbance in Area 2 as zero. Then error index of Area 1 output($\Delta f1$), i.e., ISE1 and Area 2 output($\Delta f2$), i.e., ISE2 are noted, where ISE being the integral squared error, defined below:

$$ISE1 = \int_0^{t_{sim}} (\Delta f1)^2 dt, \tag{39}$$

$$ISE2 = \int_0^{t_{sim}} (\Delta f2)^2 dt. \tag{40}$$

In general t_{sim} is chosen such that it is far greater than maximum of settling time of all the responses. Therefore in the present case t_{sim}=10 sec.
The relative effect of Area 1 disturbance on Area 2 with respect to Area 1 in percentage can be obtained as below:

$$E(\%) = \frac{ISE2}{ISE1} * 100. \tag{41}$$

The ISE1, ISE2 and E(%) values are listed in Table 2 for various disturbances. In non-integer and integer cases, the E(%) are approximately in the range of 0.3%-0.4% and 0.7%-0.8% respectively. But in case of Wen Tan method [20], the E(%) are approximately in the range of 13.8%-15.4%. From the above discussion, it can be concluded that the effect of Area 1 disturbance on Area 2 is almost negligible in both non-integer and integer cases, Fig. 14 also ratifies the same. But in case of Wen Tan, the disturbance effect on Area 2 is a significant as observed in Fig. 14. Hence, one can say that in present work the decoupling technique carried out for both non-integer and integer cases give satisfactory results.

The controllers are tested against 1% step load change in Area 1 for evaluation of performance of the controller. The performance of both integer and non-integer IMC controllers are compared with Wen Tan method [20] as shown in Fig. 15. From Fig. 15 it is noticed that the deviation in frequencies and tie line power is minimum due to load disturbance in the case of proposed controllers. And also it is noticed that the non-integer IMC controller outperforms the integer IMC controller for same interconnected thermal power system.

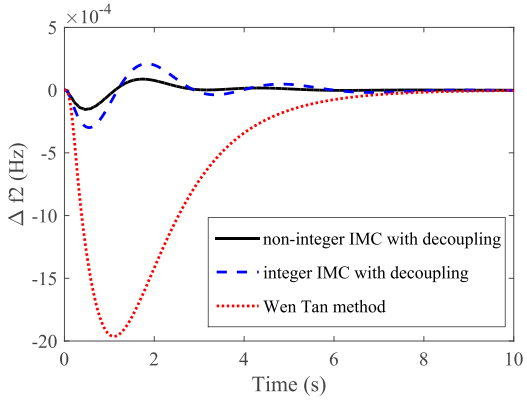

(a) $\Delta f1$.

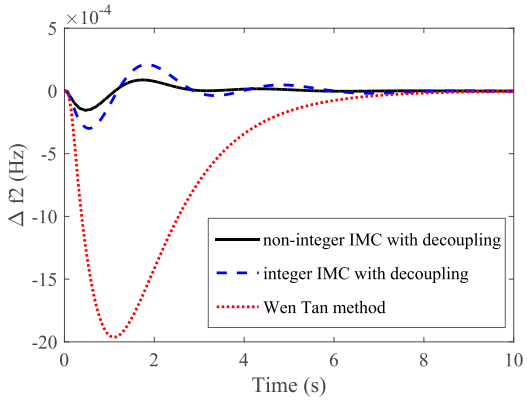

(b) $\Delta f2$.

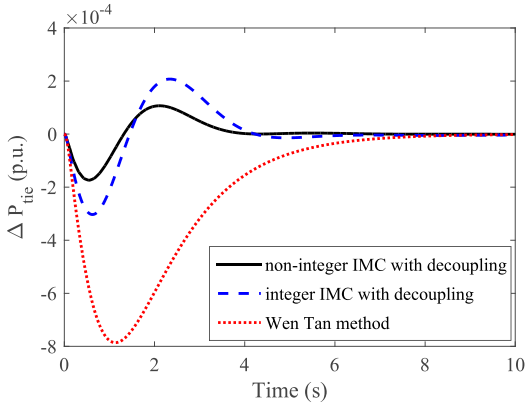

(c) ΔP_{tie}.

Fig. 13. Comparison of responses of the two area power system for lower bound uncertainties.

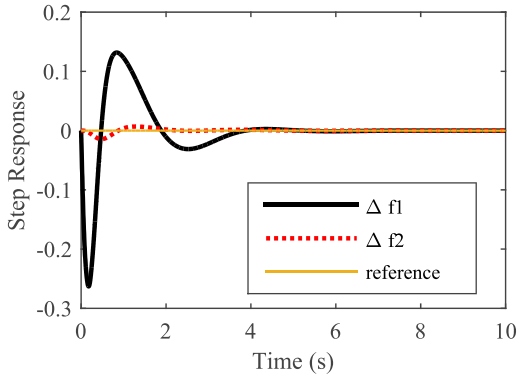

(a) Non-integer case.

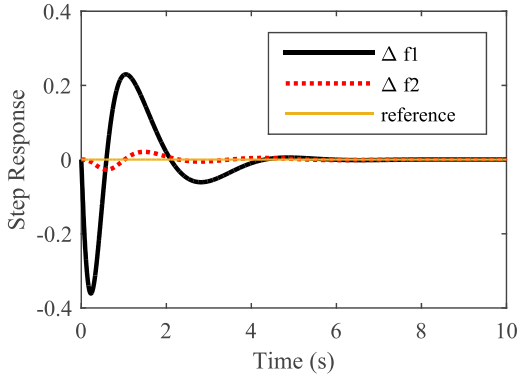

(b) Integer case.

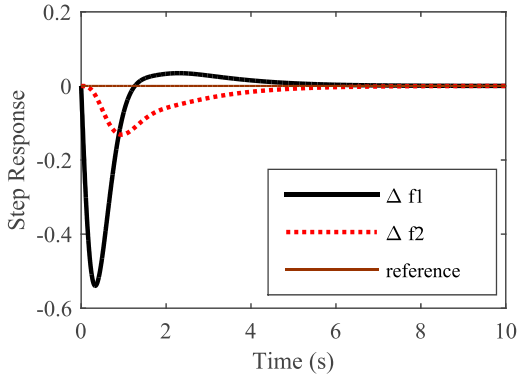

(c) Wen Tan case.

Fig. 14. Comparison of Area 1 & Area 2 responses when $\Delta P_{D1} = 0.5$ and $\Delta P_{D2} = 0$ are applied.

The dynamics of interconnected power system changes in every instant due to random load variations in load demand. So to test performance of the proposed method against random variation in load demand, the power system is simulated by applying a step load perturbation. The responses of frequency deviations in Area 1 and Area 2 and tie line power deviation are depicted in Figs. 16-18. Responses are compared with Wen Tan method [20] and it is observed that the proposed method is comparatively better, which shows the superiority of the proposed method.

The overshoot, undershoot and settling time values of frequency and tie line power deviations under step load perturbation are compared at t=20 sec and t=70 sec with Tan method, which are listed in Table 3. It is clear from Table 3 that the proposed method can minimize the effect of random changes in load demand. It is evident from Figs. 16-18 and Table 3 that proposed controllers perform

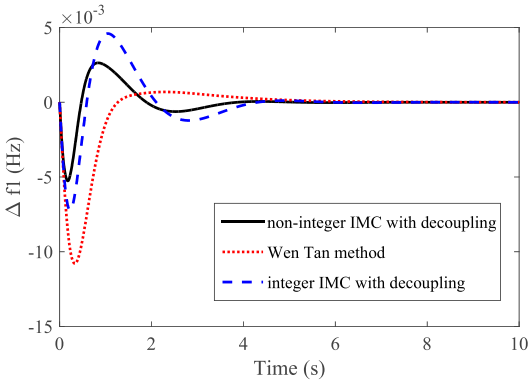

(a) $\Delta f1$.

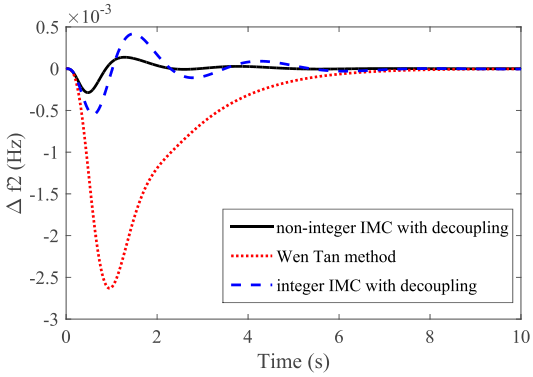

(b) $\Delta f2$.

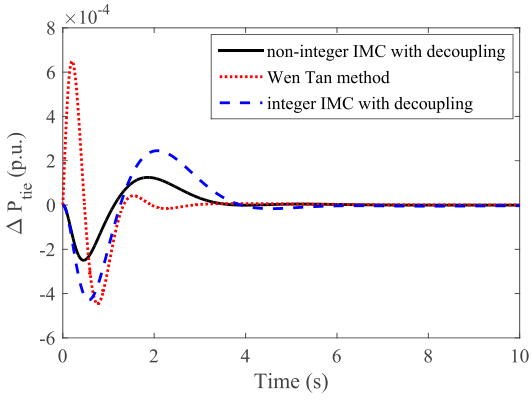

(c) ΔP_{tie}.

Fig. 15. Comparison of responses of the two area power system for 1% load change in Area 1.

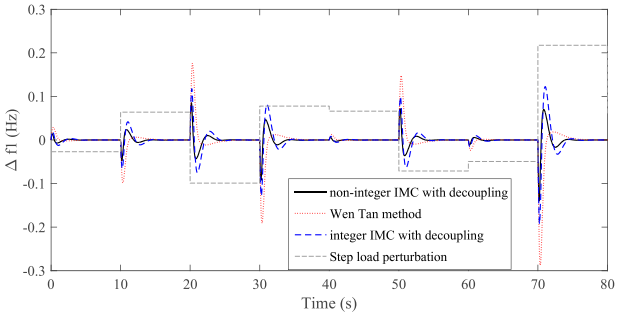

Fig. 16. Comparison of change in frequency response of first area for step load perturbation in Area 1.

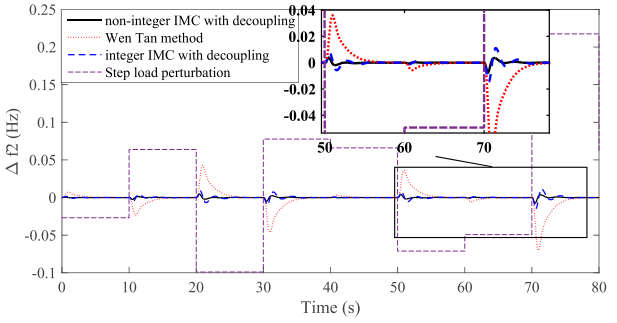

Fig. 17. Comparison of change in frequency response of second area for step load perturbation in Area 1.

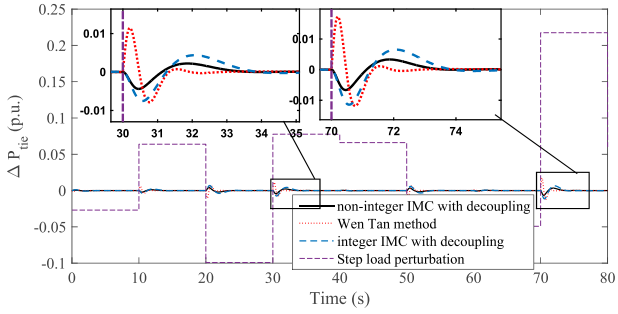

Fig. 18. Comparison of tie line power deviation for step load perturbation in Area 1.

satisfactorily when there is a change in location of the disturbance.

Testing the robustness of controller is vital because the system parameters are changed within certain specific range due to parameter estimation errors or operating point changes [41, 42]. So to test performance of the proposed controllers against uncertainty in parameters, we have chosen +50% variation called upper bound uncertainty and -50% variation called lower bound uncertainty in system parameters in each area. The uncertain parameters defined as δ_i, for all $i = 1, 2, .., 5$ are given as [15].

$$\delta_1 = \frac{1}{T_P}\varepsilon[0.00331, 0.1], \quad \delta_2 = \frac{K_P}{T_P}\varepsilon[4, 12],$$
$$\delta_3 = \frac{1}{T_T}\varepsilon[2.564, 4.762], \quad \delta_4 = \frac{1}{RT_G}\varepsilon[3.081, 10.639],$$
$$\delta_5 = \frac{1}{T_G}\varepsilon[9.615, 17.857].$$

The deviations in frequency and tie line power responses of lower and upper bound uncertainty system are depicted in Figs. 13 and 19. It is clear from Figs. 13 and

Table 3. Overshoot, undershoot and settling values for step load perturbation case.

	IMC based controller	Step load perturbation case					
		t=20sec			t=70sec		
		O_{sh}	U_{sh}	$t_s(Sec)$	O_{sh}	U_{sh}	$t_s(Sec)$
$\Delta f1$	Non-integer IMC	0.085	-0.041	3.56	0.07	-0.14	3.58
	Integer IMC	0.12	-0.08	4	0.13	-0.19	4.14
	Wen Tan method	0.18	-0.01	4.5	0.025	-0.29	4.46
$\Delta f2$	Non-integer IMC	0.0046	$-2.1*10^{-3}$	3.04	0.004	-0.0075	2.74
	Integer IMC	0.009	$-7*10^{-3}$	5.25	0.012	-0.015	5.25
	Wen Tan method	0.044	-	6.28	-	-0.07	8.9
ΔP_{tie}	Non-integer IMC	0.004	-0.002	3.51	0.003	-0.006	3.5
	Integer IMC	0.007	-0.004	5.29	0.006	-0.011	3.78
	Wen Tan method	0.0074	-0.012	3.6	0.017	-0.012	3.51

Table 4. Comparison of different performance indices under 50% uncertainty.

IMC based controllers	50% Uncertainty case							
	Lower				Upper			
	ISE	RMSE	ITSE	ITAE	ISE	RMSE	ITSE	ITAE
Wen Tan method	$7.36*10^{-5}$	$9.3*10^{-6}$	$5.96*10^{-5}$	$2.3*10^{-2}$	$8.7*10^{-6}$	$1.34*10^{-4}$	$1*10^{-5}$	$1.7*10^{-2}$
Integer IMC	$1.8*10^{-5}$	$9.04*10^{-6}$	$1.81*10^{-5}$	$1.2*10^{-2}$	$1.4*10^{-5}$	$1.05*10^{-5}$	$1.48*10^{-5}$	$1.2*10^{-2}$
Non-integer IMC	$6*10^{-6}$	$1.65*10^{-6}$	$4.72*10^{-6}$	$5.2*10^{-3}$	$4.7*10^{-6}$	$1.26*10^{-6}$	$4*10^{-5}$	$5*10^{-3}$

19, that the proposed method is robust against system parameter variations in terms of overshoot, undershoot and settling time. Table 4 shows the various performance indices like ISE, RMSE, ITSE, ITAE for lower and upper uncertainty cases. Results are compared with Wen Tan method for the same system which shows the superiority of the proposed method. Performance indices of proposed method are significantly lower than that of Tan's method. It is evident from Table 4 that performance indices of non-integer IMC controller are much smaller than integer IMC controller and Wen Tan method. Thus the non-integer IMC outperforms the integer IMC and Wen Tan method.

Finally, sensitivity analysis is carried out to examine the robustness the power system under wide changes in parameters. The system parameters such as governor time constant, turbine time constant and tie line power time constant are changing +50% to -50% in steps of 25% from their nominal values. In each simulation one parameter is varied in one area only. Likewise, all parameters are varied one at a time to test the sensitivity of the power system. The two area power system model equipped with non-integer IMC controller and a step disturbance 10% is given in Area 1. The corresponding system dynamic responses are shown in Fig. 20. It is clear from Fig. 20 that system is less sensitive to changes in T_{12} and T_G. But in case of T_T, system is more sensitive at $\pm 50\%$ change in T_T.

The technique to find the closed loop stability of such system has been discussed by Wen Tan [20]. As per the procedure, firstly the two area power system represented by Fig. 1 is rearranged as shown in Fig. 21, where M(s) is the transfer function relating ΔP_{tie} and $\Delta f_i, (i = 1,2)$ and is given below:

$$M(s) = M_1(s) - M_2(s),$$

where

$$M_1(s) = \frac{G_{P1}(s) + G_{P1}(s)G_{T1}(s)G_{G1}(s)K_1(s)}{\left(\begin{array}{l} 1 + G_{P1}(s)G_{T1}(s)G_{G1}(s)/R_1 \\ \quad + G_{P1}(s)G_{T1}(s)G_{G1}(s)K_1(s)B_1 \end{array}\right)},$$

$$M_2(s) = \frac{G_{P2}(s) + G_{P2}(s)G_{T2}(s)G_{G2}(s)K_2(s)}{\left(\begin{array}{l} 1 + G_{P2}(s)G_{T2}(s)G_{G2}(s)/R_2 \\ \quad + G_{P2}(s)G_{T2}(s)G_{G2}(s)K_2(s)B_2 \end{array}\right)},$$

and $K_1(s)$ and $K_2(s)$ are the controllers in Area 1 and Area 2 respectively.

From the Bode diagram of $M(s)/s$, one can find the stability of overall closed loop system for different cases of IMC controller like non integer IMC with decoupling, integer IMC with decoupling and Wen Tan [20] method as shown in Fig. 22. Hence, the phase margin(PM), gain margins(GM), gain cross over frequency(w_{gc}) and phase cross over frequency(w_{pc}) for different controllers are given below:

- Non-integer IMC: GM= 27.6 dB, PM= 26.2 deg, $w_{gc} = 4.3$ rad/s and $w_{pc} = 23.2$ rad/s,
- Integer IMC: GM= 22.4 dB and PM= 23.8 deg, $w_{gc} = 4.4$ rad/s and $w_{pc} = 16$ rad/s,

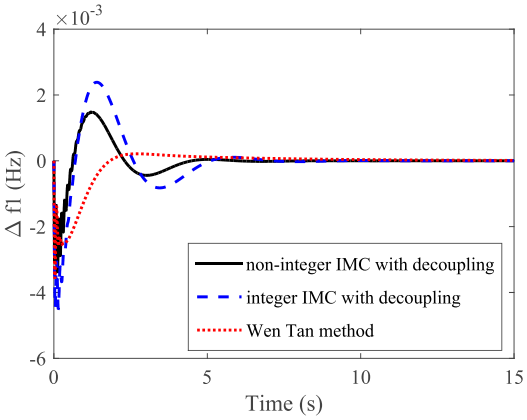

(a) $\Delta f1$.

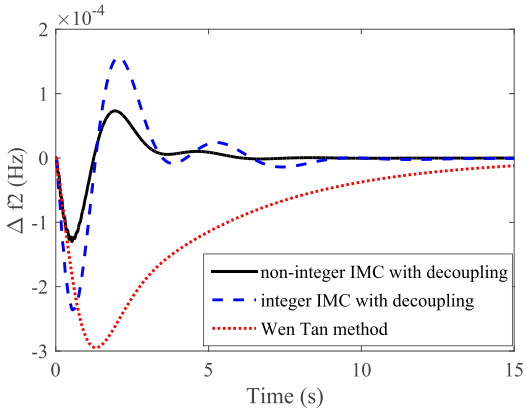

(b) $\Delta f2$.

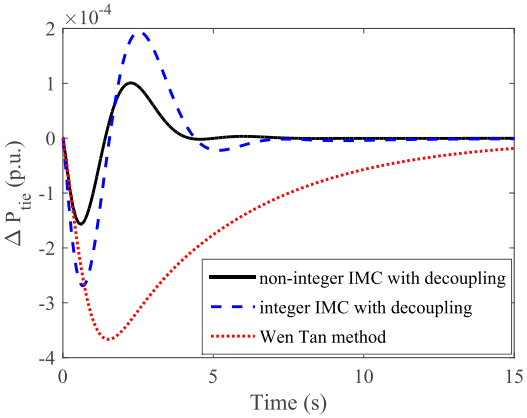

(c) ΔP_{tie}.

Fig. 19. Comparison of responses of the two area power system for upper bound uncertainties.

- Wen Tan method: GM= 8.3 dB and PM= 28.2 deg, $w_{gc} = 5.97$ rad/s and $w_{pc} = 9.45$ rad/s.

Therefore, one can conclude that the implementation of these integer IMC, non-integer IMC and Wen Tan method result in closed loop stability of the system as both GM & PM are positive and $w_{gc} < w_{pc}$ for all the cases.

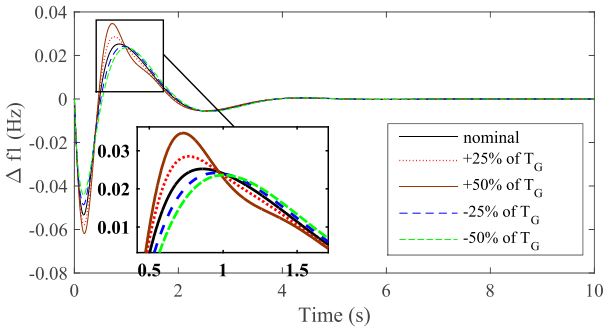

(a) $\Delta f1$ for change in T_G.

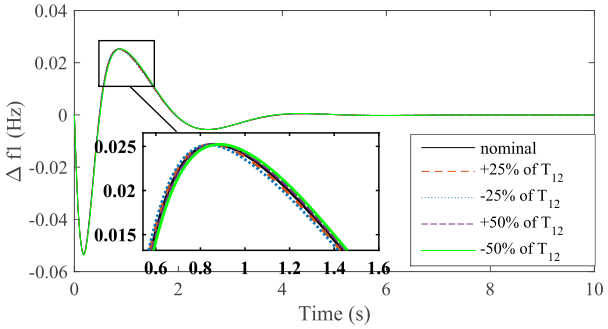

(b) $\Delta f1$ for change in T_{12}.

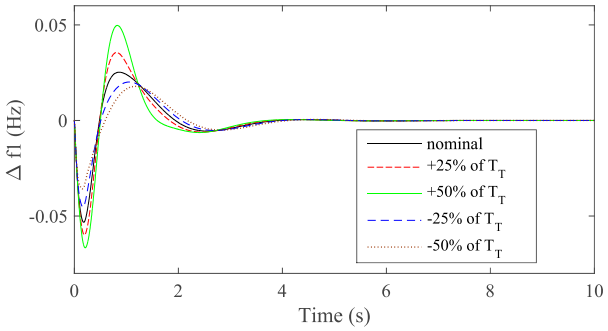

(c) $\Delta f1$ for change in T_T.

Fig. 20. Comparison of change in frequency in Area 1 for different parameter variation(non-integer case).

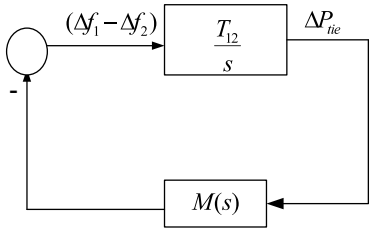

Fig. 21. Equivalent closed loop system for two area case.

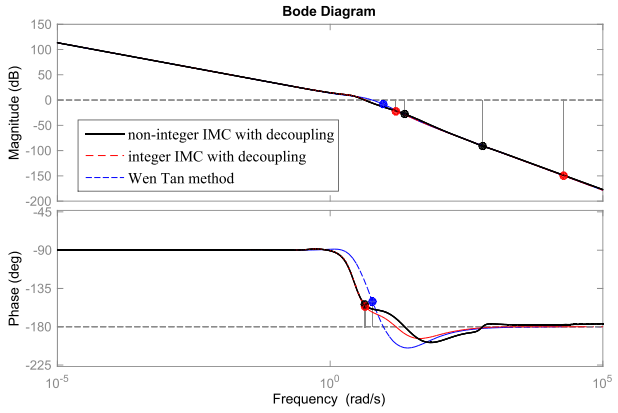

Fig. 22. Bode diagram of M/s.

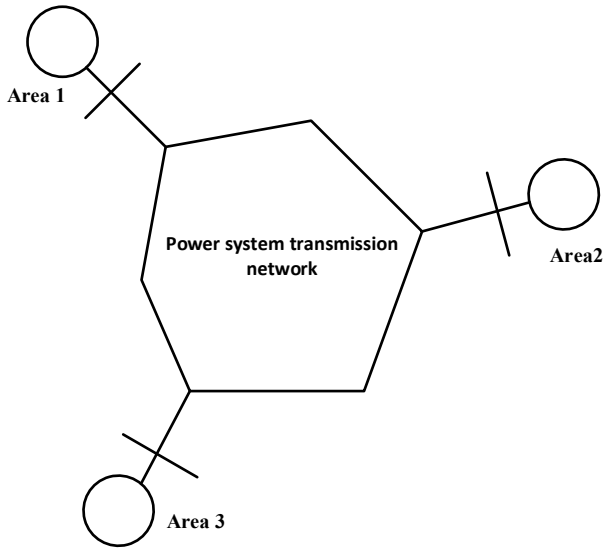

Fig. 23. A three area non reheated thermal power system [12].

5. THREE AREA EXTENSION

This section deals with the applicability of the proposed controller to a three area power system which demonstrates an extension of two area power system as shown in Fig. 23. Fig. 24 shows a block diagram for the ith area of a multi area power system.

The transfer function models for the ith area power systems are given by (42) [12].

$$G_{Gi}(s) = \frac{1}{T_{Gi}s+1}, \quad G_{Ti}(s) = \frac{1}{T_{Ti}s+1},$$
$$G_{Pi}(s) = \frac{K_{Pi}}{T_{Pi}s+1} \quad (i = 1,2,3), \tag{42}$$

where, the three area power system model parameters [12] are $T_{P1} = 20$, $T_{P2} = 25$, $T_{P3} = 20$, $T_{T1} = 0.3$, $T_{T2} = 0.33$, $T_{T3} = 0.35$, $T_{G1} = 0.08$, $T_{G2} = 0.072$, $T_{G3} = 0.07$, $K_{P1} = 120$, $K_{P2} = 112.5$, $K_{P3} = 115$, $R_1 = 2.4$, $R_2 = 2.7$, $R_3 = 2.5$, $B_1 = B_2 = B_3 = 0.416$, $T_{12} = T_{13} = T_{23} = 0.172$.

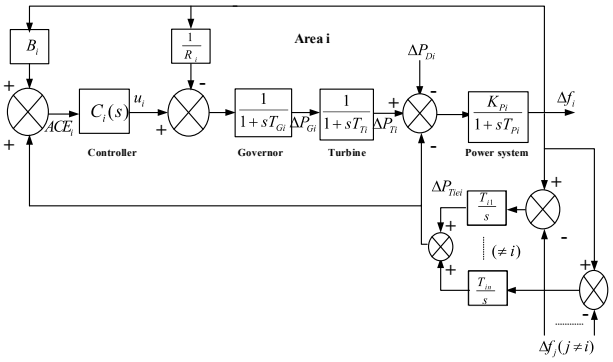

Fig. 24. Block diagram of ith area of multi area power system.

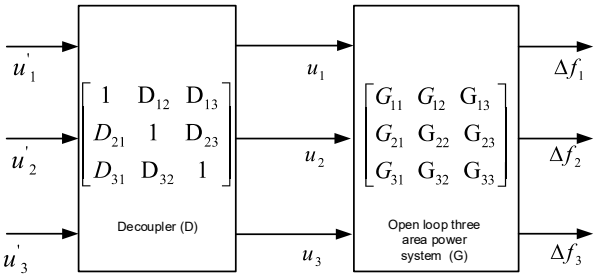

Fig. 25. A simplified decoupling of three input three output system.

As observed in two area power system the phenomenon of coupling arises among the inputs and outputs which is discussed in Section 2.2. Same problem is encountered while designing AGC for three area power system. Hence here also the interactions are decoupled among various inputs and outputs to get three SISO system for design and implementation of IMC based controller. The simplified decoupling [24, 43] of a three input three output system is shown in Fig. 25.

Consider the three input three output system and is represented by

$$G(s) = \begin{bmatrix} G_{11}(s) & G_{12}(s) & G_{13}(s) \\ G_{21}(s) & G_{22}(s) & G_{23}(s) \\ G_{31}(s) & G_{32}(s) & G_{33}(s) \end{bmatrix}. \tag{43}$$

Selecting [13] a decoupler matrix so that $G^*(s) = G(s) * D(s)$ is diagonal matrix and is given by

$$D(s) = \begin{bmatrix} 1 & D_{12}(s) & D_{13}(s) \\ D_{21}(s) & 1 & D_{23}(s) \\ D_{31}(s) & D_{32}(s) & 1 \end{bmatrix}, \tag{44}$$

where

$$D_{12}(s) = \frac{G_{13}(s)G_{32}(s) - G_{12}(s)G_{33}(s)}{G_{11}(s)G_{33}(s) - G_{13}(s)G_{31}(s)},$$

$$D_{32}(s)=\frac{G_{31}(s)G_{12}(s)-G_{32}(s)G_{11}(s)}{G_{11}(s)G_{33}(s)-G_{13}(s)G_{31}(s)},$$
$$D_{21}(s)=\frac{G_{23}(s)G_{31}(s)-G_{21}(s)G_{33}(s)}{G_{22}(s)G_{33}(s)-G_{23}(s)G_{32}(s)},$$
$$D_{31}(s)=\frac{G_{32}(s)G_{21}(s)-G_{31}(s)G_{22}(s)}{G_{22}(s)G_{33}(s)-G_{23}(s)G_{32}(s)},$$
$$D_{13}(s)=\frac{G_{12}(s)G_{23}(s)-G_{13}(s)G_{22}(s)}{G_{11}(s)G_{22}(s)-G_{12}(s)G_{21}(s)},$$
$$D_{23}(s)=\frac{G_{21}(s)G_{13}(s)-G_{23}(s)G_{11}(s)}{G_{11}(s)G_{22}(s)-G_{12}(s)G_{21}(s)}.$$

Then the resulting matrix $G^*(s)$ is obtained as

$$G^*(s)=\begin{bmatrix}G_{11}^*(s) & 0 & 0\\ 0 & G_{22}^*(s) & 0\\ 0 & 0 & G_{22}^*(s)\end{bmatrix}$$
$$=G(s)*D(s), \tag{45}$$

where $G_{11}^*(s)=G_{11}(s)+G_{12}(s)D_{21}(s)+G_{13}(s)D_{31}(s)$, $G_{22}^*(s)=G_{22}(s)+G_{21}(s)D_{12}(s)+G_{23}(s)D_{32}(s)$, $G_{33}^*(s)=G_{33}(s)+G_{31}(s)D_{13}(s)+G_{32}(s)D_{23}(s)$, where $G_{11}^*(s)$, $G_{22}^*(s)$ and $G_{33}^*(s)$ represent the SISO systems relating Area 1 input($u_1^{'}$) to Area 1 output(Δf_1), Area 2 input($u_2^{'}$) to Area 2 output(Δf_2) and Area 3 input($u_3^{'}$) to Area 3 output(Δf_3) respectively.

Here $G_{11}(s)$, $G_{22}(s)$, $G_{33}(s)$, $G_{12}(s)$, $G_{13}(s)$, $G_{23}(s)$, $G_{21}(s)$, $G_{31}(s)$ and $G_{32}(s)$ are the estimated transfer function model between Area 1 input(u_1) to Area 1 output(Δf_1), Area 2 input(u_2) to Area 2 output(Δf_2), Area 3 input(u_3) to Area 3 output(Δf_3), Area 1 input(u_1) to Area 2 output(Δf_2), Area 1 input(u_1) to Area 3 output(Δf_3), Area 2 input(u_2) to Area 3 output(Δf_3), Area 2 input(u_2) to Area 1 output(Δf_1), Area 3 input(u_3) to Area 1 output(Δf_1) and Area 3 input(u_3) to Area 2 output(Δf_2) respectively.

Following the same system identification procedure for three area power system model that has been done for two area power system as discussed in Section 2.3, the estimated transfer function models are obtained given below:

$$G_{11}(s)=\frac{(1.81s+0.8245)e^{-0.016s}}{0.1s^3+0.35s^2+1.25s+1},$$
$$G_{22}(s)=\frac{(1.9s+0.8245)e^{-0.08s}}{0.13s^3+0.465s^2+1.1625s+1},$$
$$G_{33}(s)=\frac{(1.825s+0.8245)e^{-0.016s}}{0.126s^3+0.373s^2+1.28s+1},$$
$$G_{12}(s)=\frac{(0.8245)e^{-0.232s}}{0.155s^3+0.378s^2+1.006s+1},$$
$$G_{13}(s)=\frac{(0.8245)e^{-0.168s}}{0.15s^3+0.283s^2+1.16s+1},$$
$$G_{23}(s)=\frac{(0.8245)e^{-0.261s}}{0.154s^3+0.354s^2+0.964s+1},$$
$$G_{21}(s)=\frac{(0.8245)e^{-0.184s}}{0.18s^3+0.4s^2+1.1s+1},$$
$$G_{31}(s)=\frac{(0.8245)e^{-0.31s}}{0.11s^3+0.25s^2+s+1},$$
$$G_{32}(s)=\frac{(0.8245)e^{-0.099s}}{0.23s^3+0.41s^2+1.2s+1}.$$

The corresponding RMSE values of estimated models are obtained as 0.08, 0.03, 0.052, 0.021, 0.028, 0.022, 0.025, 0.013 and 0.041.

Substituting the systems $G_{11}(s)$, $G_{22}(s)$, $G_{33}(s)$, $G_{12}(s)$, $G_{13}(s)$, $G_{23}(s)$, $G_{21}(s)$, $G_{31}(s)$ and $G_{32}(s)$ in (42), then elements $G_{11}^*(s)$, $G_{22}^*(s)$ and $G_{33}^*(s)$ of $G^*(s)$ are simplified as

$$G_{11}^*(s)=\frac{(0.2869s^2+16.06s+0.04)e^{-0.038s}}{s^3+2.77s^2+10.25s+6.64},$$
$$G_{22}^*(s)=\frac{(0.009s^2+15.9s+0.01)e^{-0.04s}}{s^3+3.33s^2+8.31s+6.2},$$
$$G_{33}^*(s)=\frac{(0.197s^2+13.47s+0.001)e^{-0.043s}}{s^3+2.37s^2+8.6s+5.23}.$$

Adopting IMC design procedure to $G_{11}^*(s)$, $G_{22}^*(s)$ and $G_{33}^*(s)$, we have integer and non-integer IMC controllers are given by (46) and (47)

$$C_i(s)=K_{int}(s)=\frac{Q_i(s)Q_{di}(s)}{1-\bar{P}(s)Q_i(s)Q_{di}(s)},\quad i=1,2,3, \tag{46}$$

where i is the ith area power system.

Area 1:

$$Q_1(s)=\frac{s^3+2.77s^2+10.25s+6.64}{(0.2869s^2+16.06s+0.04)(0.06s+1)},$$
$$Q_{d1}(s)=\frac{0.18961s+1}{(0.13s+1)},$$

and $\bar{P}(s)=G_{11}^*(s)$.

Area 2:

$$Q_2(s)=\frac{s^3+3.33s^2+8.31s+6.2}{(0.009s^2+15.9s+0.01)(0.1s+1)},$$
$$Q_{d2}(s)=\frac{0.299s+1}{(0.2s+1)},$$

and $\bar{P}(s)=G_{22}^*(s)$.

Area 3:

$$Q_3(s)=\frac{s^3+2.37s^2+8.6s+5.23}{(0.197s^2+13.47s+0.001)(0.05s+1)},$$
$$Q_{d3}(s)=\frac{0.1996s+1}{(0.15s+1)},$$

and $\bar{P}(s)=G_{33}^*(s)$.

$$C_i(s)=K_{non-int}(s)$$
$$=\frac{Q_i(s)Q_{di}(s)}{1-\bar{P}(s)Q_i(s)Q_{di}(s)},\quad i=1,2,3, \tag{47}$$

where i is the i^{th} area power system.

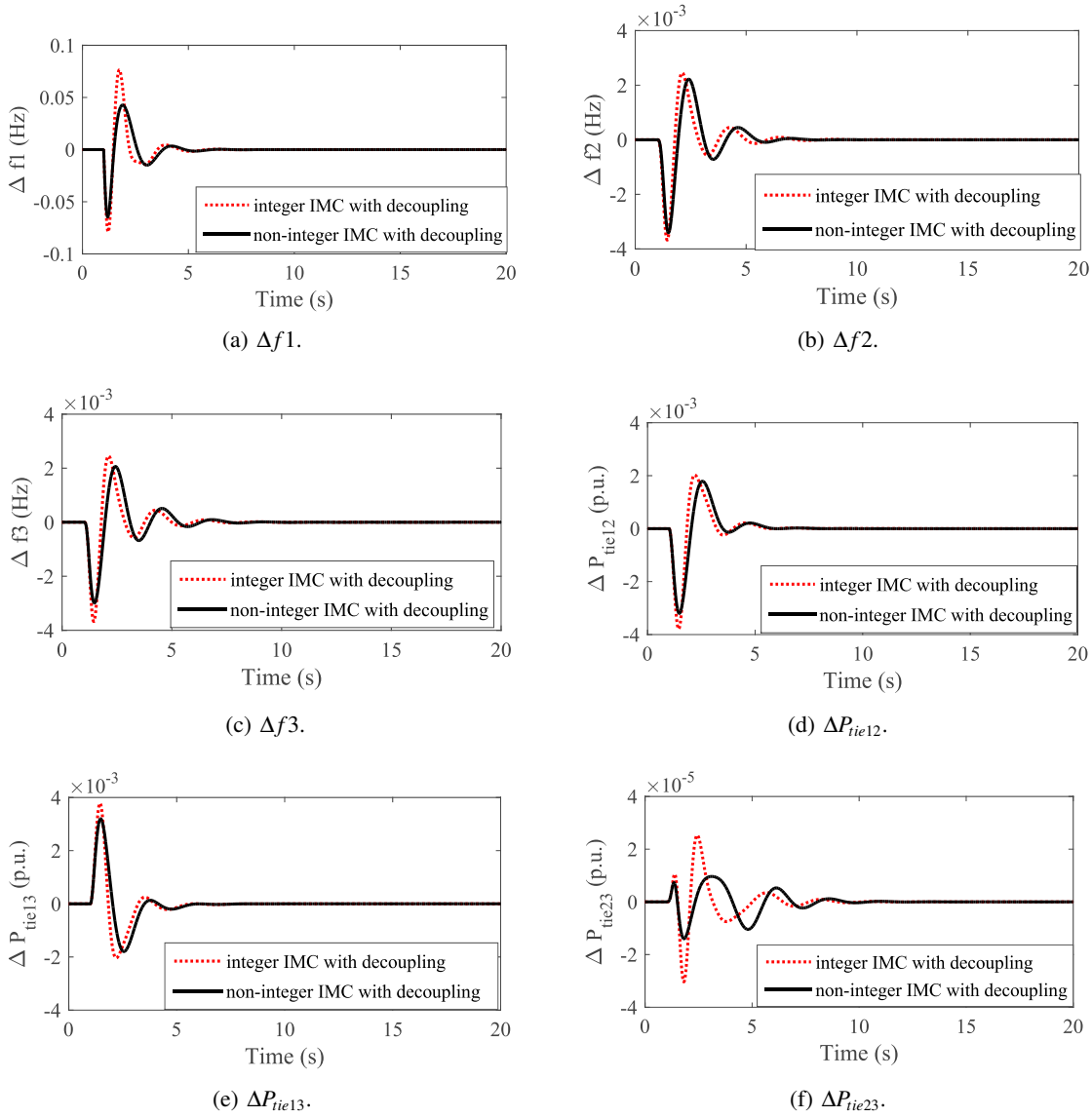

(a) $\Delta f1$. (b) $\Delta f2$.

(c) $\Delta f3$. (d) ΔP_{tie12}.

(e) ΔP_{tie13}. (f) ΔP_{tie23}.

Fig. 26. Responses of the three area power system.

Area 1:

$$Q_1(s) = \frac{s^3 + 2.77s^2 + 10.25s + 6.64}{(0.2869s^2 + 16.06s + 0.04)(0.06s^{1.05} + 1)},$$
$$Q_{d1}(s) = \frac{0.09s + 1}{(0.1s^{1.02} + 1)},$$

and $\bar{P} = G^*_{11}(s)$.

Area 2:

$$Q_2(s) = \frac{s^3 + 3.33s^2 + 8.31s + 6.2}{(0.009s^2 + 15.9s + 0.01)(0.05s^{1.06} + 1)},$$
$$Q_{d2}(s) = \frac{0.143s + 1}{(0.12s^{1.02} + 1)},$$

and $\bar{P} = G^*_{22}(s)$.

Area 3:

$$Q_3(s) = \frac{s^3 + 2.37s^2 + 8.6s + 5.23}{(0.197s^2 + 13.47s + 0.001)(0.01s^{1.09} + 1)},$$
$$Q_{d3}(s) = \frac{0.141s + 1}{(0.15s^{1.02} + 1)},$$

and $\bar{P} = G^*_{33}(s)$.

The controllers are tested against 10% step load change at $t = 1$ sec in Area 1 for evaluation of performance of the controllers. The dynamic responses of the three area non-reheated thermal power system are shown Fig. 26. It is observed that proposed controllers performs satisfactorily when there is a load change in power system. Also it is evident from Fig. 26 that non-integer IMC controller performance is better than integer IMC controller.

6. CONCLUSION

In the present work, a two area non-reheated thermal power system is considered to demonstrates the proposed method. The idea of simplified decoupling technique is introduced to decouple the power system into equivalent SISO models for decentralised controller design. Both integer and non-integer IMC based LFC controller are designed for the obtained decoupled SISO models. Robustness and performance of the controlled system are tested using MATLAB simulation. The simulation results show that the proposed method is robust and has good tracking characteristics as it minimizes the effect of disturbance. The superiority of both proposed controllers over Wen Tan method is shown by comparative study. Among the two proposed controllers, it is observed that non-integer IMC outperforms integer IMC. The proposed method when applied for the design of AGC for a three area powers system, found to be satisfactory.

REFERENCES

[1] P. Kundur, *Power System Stability and Control*, TMH 8th reprint, New Delhi, 2009.

[2] M. Eremia and M. Shahidehpour, Eds., *Handbook of Electrical Power System Dynamics: Modeling, Stability, and Control*, ser. IEEE Press Series on Power Engineering, Hoboken, IEEE Press/Wiley, New Jersey, 2013.

[3] O.I.Elgerd, *Electric Energy Systems Theory. An Introduction*, TMH, New Delhi, 1983.

[4] Ibraheem, P. Kumar, and D. P. Kothari, "Recent philosophies of automatic generation control strategies in power systems," *IEEE Transactions on Power Systems*, vol. 20, no. 1, pp. 346-357, Feb 2005. [click]

[5] S. K. Pandey, S. R. Mohanty, and N. Kishor, "A literature survey on load frequency control for conventional and distribution generation power systems," *Renewable and Sustainable Energy Reviews*, vol. 25, pp. 318-334, 2013. [click]

[6] H. Bevrani and T. Hiyama, "Robust decentralised pi based lfc design for time delay power systems," *Energy Conversion and Management*, vol. 49, no. 2, pp. 193-204, 2008. [click]

[7] H. Shayeghi, H. Shayanfar, and O. Malik, "Robust decentralized neural networks based lfc in a deregulated power system," *Electric Power Systems Research*, vol. 77, no. 3-4, pp. 241-251, 2007. [click]

[8] S. Saxena and Y. V. Hote, "Decentralized pid load frequency control for perturbed multi-area power systems," *International Journal of Electrical Power and Energy Systems*, vol. 81, pp. 405-415, 2016.

[9] W. Tan and H. Zhou, "Robust analysis of decentralized load frequency control for multi-area power systems," *International Journal of Electrical Power and Energy Systems*, vol. 43, no. 1, pp. 996-1005, 2012.

[10] H. A. Yousef, K. AL-Kharusi, M. H. Albadi, and N. Hosseinzadeh, "Load frequency control of a multi area power system: An adaptive fuzzy logic approach," *IEEE Transactions on Power Systems*, vol. 29, no. 4, pp. 1822-1830, Jul. 2014.

[11] Y. Mi, Y. Fu, C. Wang, and P. Wang, "Decentralized sliding mode load frequency control for multi area power systems," *IEEE Transactions on Power Systems*, vol. 28, no. 4, pp. 4301-4309, Nov. 2013. [click]

[12] M. Zribi, M. Al-Rashed, and M. Alrifai, "Adaptive decentralized load frequency control of multi-area power systems," *International Journal of Electrical Power and Energy Systems*, vol. 27, no. 8, pp. 575-583, 2005.

[13] B. Bequette, *Process Control: Modeling, Design, and Simulation*, ser. Prentice-Hall International Se., Prentice Hall PTR, 2003.

[14] S. Saxena and Y. V. Hote, "Internal model control based pid tuning using first-order filter," *International Journal of Control, Automation and Systems*, vol. 15, no. 1, pp. 149-159, Feb 2017. [click]

[15] Wen Tan, "Unified tuning of pid load frequency controller for power systems via imc," *IEEE Transactions on Power Systems*, vol. 25, no. 1, pp. 341-350, Feb. 2010. [click]

[16] S. Saxena and Y. V. Hote, "Load frequency control in power systems via internal model control scheme and model order reduction," *IEEE Transactions on Power Systems*, vol. 28, no. 3, pp. 2749-2757, Aug. 2013. [click]

[17] A. Mujumdar, B. Tamhane, and S. Kurode, "Observer-Based Sliding Mode Control for a Class of Noncommensurate Fractional-Order Systems," *IEEE/ASME Transactions on Mechatronics*, vol. 20, no. 5, pp. 2504-2512, Oct. 2015.

[18] H. Benlaoukli, D. Nelson-Gruel, P. Lanusse, and A. Oustaloup, "Fractional-order control and interval analysis of siso systems with time-delayed state," *IET Control Theory & Applications*, vol. 2, no. 1, pp. 16-23, Jan. 2008.

[19] I. Pan and S. Das, "Fractional order agc for distributed energy resource using robust optimization," *IEEE Transactions on Smart Grid*, vol. 7, no. 5, pp. 2175-2186, Sep. 2016. [click]

[20] W. Tan, "Tuning of pid load frequency controller for power systems," *Energy Conversion and Management*, vol. 50, no. 6, pp. 1465-1472, 2009.

[21] A. Tepljakov, E. Petlenkov, and J. Belikov, "Fomcon: Fractional-order modeling and control toolbox for matlab," *Proceedings of the 18th International Conference Mixed Design of Integrated Circuits and Systems - MIXDES 2011*, June 2011, pp. 684-689.

[22] A. Y. Sivaramakrishnan, M. V. Hariharan, and M. C. Srisailam, "Design of variable-structure load-frequency controller using pole assignment technique," *International Journal of Control*, vol. 40, no. 3, pp. 487-498, 1984. [click]

[23] E. Ali and S. Abd-Elazim, "Bacteria foraging optimization algorithm based load frequency controller for interconnected power system," *International Journal of Electrical Power and Energy Systems*, vol. 33, no. 3, pp. 633 - 638, 2011. [click]

[24] W. L. Luyben, "Distillation decoupling," *AIChE Journal*, vol. 16, no. 2, pp. 198-203, 1970. [click]

[25] C. Shi, X. Wang, S. Wang, J. Wang, and M. M. Tomovic, "Adaptive decoupling synchronous control of dissimilar redundant actuation system for large civil aircraft," *Aerospace Science and Technology*, vol. 47, pp. 114-124, 2015.

[26] L. Linh, T. N. L. Vu, and L. H. Giang, "Design of imc-pid controller cascaded filter for simplified decoupling control system," *International Journal of Electrical, Computer, Energetic, Electronic and Communication Engineering*, vol. 10, no. 7, pp. 887-902, 2016.

[27] X. Wang, C. Shi, and S. Wang, "Extended state observer-based motion synchronisation control for hybrid actuation system of large civil aircraft," *International Journal of Systems Science*, vol. 48, no. 10, pp. 2212-2222, 2017. [click]

[28] E. Gagnon, A. Pomerleau, and A. Desbiens, "Simplified, ideal or inverted decoupling," *ISA Transactions*, vol. 37, no. 4, pp. 265-276, 1998. [click]

[29] T. O. R. A. A. Tohme, Elie ; Poinot, "Initialization of output error identification algorithms," Ph.D. dissertation, 2008, phD thesis Automatique Balamand, Liban 2008.

[30] A. C. Supriyadi, H. Takano, J. Murata, and T. Goda, "Adaptive robust pss to enhance stabilization of interconnected power systems with high renewable energy penetration," *Renewable Energy*, vol. 63, pp. 767-774, 2014. [click]

[31] G. P. Rao and H. Unbehauen, "Identification of continuous-time systems," pp. 185-220, March 2006.

[32] A. Fujimori and S. Ohara, "Order reduction of plant and controller in closed loop identification based on joint input-output approach," *International Journal of Control, Automation and Systems*, vol. 15, no. 3, pp. 1217-1226, Jun 2017.

[33] I. Saaki, P. C. Babu, C. K. Rao, and D. S. Prasad, "Integral square error minimization technique for linear multi input and multi output systems," *Proceedings of International Conference on Power and Energy Systems*, pp. 1-5, Dec 2011.

[34] T. Soderstrom and P. Stoica, *System Identification*, ser. Prentice Hall International Series In Systems And Control Engineering, Prentice Hall, 1989.

[35] J. Holland, *Adaptation in Natural and Artificial Systems: An Introductory Analysis with Applications to Biology, Control, and Artificial Intelligence*, University of Michigan Press, 1975.

[36] J. Lee, W. Chung, E. Kim, and S. Kim, "A new genetic approach for structure learning of bayesian networks: Matrix genetic algorithm," *International Journal of Control, Automation and Systems*, vol. 8, no. 2, pp. 398-407, 2010. [click]

[37] M. Ismail, M. Moghavvemi, and T. Mahlia, "Genetic algorithm based optimization on modeling and design of hybrid renewable energy systems," *Energy Conversion and Management*, vol. 85, pp. 120-130, Sep. 2014. [click]

[38] H. Lee, H. Lee, and E. Kim, "A new gait recognition system based on hierarchical fair competition-based parallel genetic algorithm and selective neural network ensemble," *International Journal of Control, Automation and Systems*, vol. 12, no. 1, pp. 202-207, Feb 2014.

[39] D. E. Rivera, M. Morari, and S. Skogestad, "Internal model control: PID controller design," *Industrial & Engineering Chemistry Process Design and Development*, vol. 25, no. 1, pp. 252-265, 1986.

[40] M. Morari and E. Zafiriou, *Robust Process Control*, Prentice Hall, 1989.

[41] L. C. Saikia, J. Nanda, and S. Mishra, "Performance comparison of several classical controllers in agc for multi-area interconnected thermal system," *International Journal of Electrical Power and Energy Systems*, vol. 33, no. 3, pp. 394-401, 2011. [click]

[42] K. S. Parmar, S. Majhi, and D. Kothari, "Load frequency control of a realistic power system with multi-source power generation," *International Journal of Electrical Power and Energy Systems*, vol. 42, no. 1, pp. 426 - 433, 2012.

[43] T. N. L. Vu and M. Lee, "Design of extended simplified decoupling for multivariable processes with multiple time delays," *Proceedoings of 11th International Conference on Control, Automation and Systems*, Oct 2011, pp. 1822-1827.

Idamakanti Kasireddy received the M.Tech. degree from National Institute of Technology, Jamshedpur, India,in 2015. He is currently working towards the Ph.D. degree at the Department of Electrical and Electronics Engineering, NIT Jamshedpur, India. His research interests include integer & non-integer modelling and different control strategies in power and energy systems.

Abdul Wahid Nasir received the M.Tech. degree from Crescent University, Chennai, India, in 2014. He is currently working as a research scholar in the Department of Electrical & Electronics Engineering, NIT Jamshedpur, Jharkhand, India. His research interests include application of fractional order systems and control in different areas of control engineering.

Arun Kumar Singh received his B.Sc. degree from NIT kurukshetra, Haryana, India, an M.Tech. degree from the IIT (BHU), Varanasi, UP, India, and a Ph.D. degree from the IIT Kharagpur, India. He has been a professor in the Department of Electrical and Electronics Engineering at NIT Jamshedpur, since 1985. His research interests include application of optimization algorithms, integer & non-integer modelling and different control strategies in power and energy systems.